Available online at www.sciencedirect.com
ScienceDirect
Journal of Solid State Chemistry 180 (2007) 2356–2362
JOURNAL OF SOLID STATE CHEMISTRY
www.elsevier.com/locate/jssc

Structure, and magnetic and transport behavior of twinned $Ce_2Rh_3(Pb,Bi)_5$

Evan Lyle Thomas[a,1], Moo Sung Kim[b], D.A. Sokolov[b], Marcus C. Bennett[b], M.C. Aronson[b], Julia Y. Chan[a,*]

[a]Department of Chemistry, Louisiana State University, 232 Choppin Hall, Baton Rouge, LA 70803, USA
[b]Department of Physics, 2477 Randall Laboratory, University of Michigan, 500 East University Avenue, Ann Arbor, MI 48109, USA

Received 14 April 2007; received in revised form 15 June 2007; accepted 16 June 2007
Available online 22 June 2007

Abstract

Single crystals of a new compound, $Ce_2Rh_3(Pb,Bi)_5$, have been grown via a flux-growth technique using molten Pb as a solvent. The compound has been characterized by single crystal X-ray diffraction and found to be of the orthorhombic $Y_2Rh_3Sn_5$ structure type [$Cmc2_1$ (No. 36), $Z=4$] with lattice parameters $a=4.5980(2)$, $b=27.1000(17)$ and $c=7.4310(4)$ Å, with $V=925.95(9)$ Å^3. $Ce_2Rh_3(Pb,Bi)_5$ has a complex crystal structure containing Ce atoms encased in Rh–X (X = Pb/Bi) pentagonal and octagonal channels in [100], with polyanions similar to those found in $Ce_2Au_3In_5$ and $Yb_2Pt_3Sn_5$. Magnetization measurements find that $Ce_2Rh_3(Pb,Bi)_5$ is a quasi-two-dimensional system, where the Ce moments are spatially well-localized. Heat capacity measurements show a transition at the Néel temperature of 1.5 K. Evidence for Fermi surface nesting is found in electrical resistivity measurements, and we argue that $Ce_2Rh_3(Pb,Bi)_5$ is very near a metal–insulator transition in zero field.

Keywords: Flux growth; Single crystal; X-ray diffraction; Twinning; CeRhBi; $Ce_2Rh_3Bi_5$; $Ce_2Rh_3(Pb,Bi)_5$; $Y_2Rh_3Sn_5$; Polyanion; Bismuthide; Electrical resistivity; Specific heat; Quasi-two dimensionality

1. Introduction

In many ternary intermetallic systems, *RE*–*T*–*X* (*RE*-rare-earth, T = transition metal, X = main group element), the hybridization between the localized *f*-electrons of rare-earth elements, and the itinerant conduction *d*-electrons supplied by surrounding atoms, leads to extraordinary physical phenomena. As a result, several ternary rare-earth intermetallic compounds with the composition $RE_2T_3X_5$ (T = Mn, Fe, Co, Ni, Ru, Rh, Os, Ir, Pt or Au; X = Al, Si, Ga, Ge, In, Sn) have been subjected to much investigation including neutron diffraction [1–5] and thermopower experiments [6], particularly those containing silicon. These compounds are shown to exhibit a variety of appealing physical property behavior including superconductivity [7–10], the coexistence of magnetism and superconductivity [11], along with valence fluctuations [6,12,13], Kondo behavior [14], and large positive magnetoresistance [15,16]. In addition, a few of these compounds are reported to have moderately enhanced values of the linear Sommerfeld coefficient (γ) of the electronic specific heat, which at low temperatures are on the order 10^2 mJ mol^{-1} K^{-2} as a result of strong coupling between the conduction- and *f*-electrons [17–19]. $Ce_2Rh_3Sn_5$ [10] and $Yb_2Pt_3Sn_5$ [20] are both moderate heavy fermion compounds, with mixed-valence behavior in the latter. $Yb_2Fe_3Si_5$ is a Kondo lattice system and also a heavy fermion with $\gamma\sim500$ mJ mol^{-1} K^{-2} [14].

A rather large number of compounds have been identified with the $RE_2T_3X_5$ formula. In addition, several structure types have been reported within this family of compounds. Each of these layered, parent "2–3–5"

*Corresponding author. Fax: +1 225 578 3458.
E-mail address: jchan@lsu.edu (J.Y. Chan).
[1]Current address: National Institute of Standards and Technology, Ceramics Division, Materials Science and Engineering Laboratory, 100 Bureau Drive MS 8520, Gaithersburg, MD 20899, USA.

0022-4596/$ - see front matter © 2007 Elsevier Inc. All rights reserved.
doi:10.1016/j.jssc.2007.06.012

structure types is derived from the tetragonal ($I4/mmm$, No. 139) $BaAl_4$ structure type. It is worthwhile to mention that a number of structural stability studies performed within these 2–3–5 systems often show a difference in the structure type adopted for the early and late rare-earth analogs. Compounds of the $Sc_2Fe_3Si_5$- [21] or $U_2Mn_3Si_5$-type adopt a tetragonal ($P4/mnc$, No. 140) structure, while compounds of the $U_2Co_3Si_5$- [22] or $Sc_2Co_3Si_5$-type ($Ibam$, No. 72) are orthorhombic. [Note that the $RE_2Co_3Si_5$ (RE = Tb, Dy) compounds crystallize with the monoclinic ($C2/c$, No. 15) $Lu_2Co_3Si_5$ structure [23] which is a structural deformation variant of the $U_2Co_3Si_5$ structure.] Isomorphs of $Yb_2Ir_3Ge_5$ crystallize in the orthorhombic space group $Pmmn$ (No. 59) [24]. The indides $Ln_2Au_3In_5$ (Ln = Ce, Pr, Nd, Sm) crystallize with the orthorhombic $Ce_2Au_3In_5$ structure ($Pmn2_1$, No. 31) [25]. The remaining 2–3–5 members crystallize with either of the orthorhombic $Y_2Rh_3Sn_5$-type [26] ($Cmc2_1$, No. 36) or $Yb_2Pt_3Sn_5$-type [27] ($Pnma$, No. 62) structures. Here, we report, to the best of our knowledge, the first Pb/Bi-containing member of this class of structurally related 2–3–5 compounds. In light of the interesting magnetic and transport behavior which has been observed in other 2–3–5 intermetallic systems, a study of the synthesis, crystal structure, magnetization, specific heat and electrical resistivity data for $Ce_2Rh_3(Pb, Bi)_5$ is presented.

2. Experimental

2.1. Synthesis and elemental composition analysis

Single crystals of $Ce_2Rh_3(Pb,Bi)_5$ were grown from a Pb flux, using equal proportions of high purity Rh and Bi from Alfa Aesar, and Ce from Ames Laboratory (>99.99%). The black crystals form with a needle-like morphology. Due to the similar scattering of Pb and Bi, X-ray measurements alone cannot distinguish these elements. Electron microprobe analysis was carried out on polished single crystals using a Cameca SX100 microprobe system with elemental standards. The stoichiometry was found to be uniform over the entire crystal surface, and also within ~2% over the crystal interior, and confirmed to be $Ce_2Rh_3Pb_4Bi$.

2.2. Structure determination by X-ray diffraction

Structure determination was performed by collecting single crystal intensity data at room temperature on a Nonius Kappa CCD X-ray diffractometer equipped with graphite monochromatized Mo$K\alpha$ radiation with $\lambda = 0.71073$ Å. A suitable sized fragment ($\sim 0.25 \times 0.05 \times 0.05\,mm^3$) from an irregularly shaped, black crystal of $Ce_2Rh_3(Pb,Bi)_5$ was mechanically selected and glued to the tip of a goniometer glass fiber. Lattice parameters were obtained from a scan in 15° φ. Integration of the data was done using DENZO [28] and the structure was solved and refined using the SHELXL software package [29]. Crystallographic, data collection and refinement parameters are given in Table 1.

Since X-ray diffraction measurements do not distinguish between $Ce_2Rh_3Pb_4Bi$ and $Ce_2Rh_3Bi_5$, for simplicity we have solved the structure of a hypothetical $Ce_2Rh_3Bi_5$ using direct methods with SIR97 [30], without independent constraints on the stoichiometry or knowledge of related structures. Non-centrosymmetric $Cmc2_1$ (No. 36), a subgroup of supergroup $Cmcm$ (No. 63), was chosen as the likely space group based on intensity statistics. This resulted in two Ce sites, three Rh sites, and five Bi sites, all on 4a Wyckoff positions. The initial structural model for $Ce_2Rh_3Bi_5$ was generated from an automatic interpretation of direct methods. Later, the atomic positions reported for the isostructural and parent compound $Y_2Rh_3Sn_5$ [26], were used in subsequent refinement procedures.

A correction for absorption was made to the experimental intensity data along with the application of a weighting scheme and the anisotropic refinement of the atomic displacement parameters. Before an extinction coefficient could be calculated, a twinning by inversion was observed. The *translationengleiche* symmetry reduction (index 2) from space group $Cmcm$ to the first-order variant $Cmc2_1$ is responsible for this occurrence. Twin refinement used the matrix ($\bar{1}00$, $0\bar{1}0$, $00\bar{1}$), and the twin fraction was

Table 1
Crystallographic and refinement data for $Ce_2Rh_3Bi_5$[a]

Formula	$Ce_2Rh_3Bi_5$
Formula weight ($g\,mol^{-1}$)	1633.869
Crystal system	Orthorhombic
Space group	$Cmc2_1$ (No. 36)
a (Å)	4.5980(2)
b (Å)	27.1000(17)
c (Å)	7.4310(4)
V (Å^3)	925.95(9)
Z	4
Crystal dimensions (mm^3)	$0.03 \times 0.05 \times 0.05$
Temperature (K)	298(2)
Crystal density ($g\,cm^{-3}$)	11.720
θ range (deg.)	2.74–30.06
μ (mm^{-1})	109.367
Collected reflections	1348
Unique reflections	733
R_{int}	0.0611
h	$-6 \rightarrow 6$
k	$-37 \rightarrow 38$
l	$-10 \rightarrow 10$
Extinction coefficient	0.00073(5)
Data/parameters/restraints	1348/63/1
T_{max}, T_{min}	0.1707, 0.0734
$R[F_o^2 > 2\sigma(F_o^2)]$[b], all data	0.0386, 0.0427
$R_w(F_o^2)$[c], all data	0.0860, 0.0892
$\Delta\rho_{max,\ min}$ (e Å^{-3})	5.486, −3.296
S (goodness of fit on F_o^2)	1.066

[a]Hypothetical structural data. See text for details.
[b]$R(F) = \sum||F_O| - |F_C||/\sum|F_O|$.
[c]$R_w(F_o^2)[\sum[w(F_O^2 - F_C^2)^2]/\sum[w(F_O^2)^2]]^{1/2}$;
$w = 1/[\sigma^2(F_o^2) + (0.0372P)^2 + 50.3837P]$, where $P = (F_o^2 + 2F_c^2)/3$.

found to be 51.5:48.5. A final full-matrix least squares on F^2 cycle was done following the calculation of an extinction coefficient. No deviation from the ideal formula $Ce_2Rh_3Bi_5$ was observed, nor was any obvious extra crystallographic symmetry detected in the presented model. A final $R[F_o^2 > 2\sigma(F_o^2)]$ of 0.0386 was obtained and the Fourier difference map revealed residual peaks of 5.486 and −3.296. The atomic parameters and bond distances for $Ce_2Rh_3Bi_5$ are listed in Tables 2 and 3, respectively.

2.3. Physical property measurements

The magnetization for a single crystal of $Ce_2Rh_3(Pb,Bi)_5$ was measured at several temperatures, and with fields both parallel and perpendicular to the needle axis. These measurements were carried out using a Quantum Design Magnetic Property Measurement System in fields as large as 7 T. The heat capacity of a single crystal was measured using a Quantum Design Physical Property Measurement system (PPMS) at temperatures between 0.4 and 20 K. The electrical resistivity was measured in the standard four-probe configuration for temperatures between 0.4 and 40 K using the quantum design PPMS.

Table 2
Atomic positions, Wyckoff site symmetry and displacement parameters for $Ce_2Rh_3Bi_5$[a]

Atom	Wyckoff position	x	y	z	U_{eq}[b]
Ce1	4*a*	0	0.17144(6)	0.7743(2)	0.0130(3)
Ce2	4*a*	0	0.47465(6)	0.7413(2)	0.0114(3)
Rh1	4*a*	0	0.05006(9)	0.5262(3)	0.0113(5)
Rh2	4*a*	0	0.77725(7)	0.7783(3)	0.0116(5)
Rh3	4*a*	0	0.39533(10)	0.4897(4)	0.0138(5)
Bi1	4*a*	0	0.87844(4)	0.74940(16)	0.0138(3)
Bi2	4*a*	0	0.71017(4)	0.48847(14)	0.0116(3)
Bi3	4*a*	0	0.59599(4)	0.61603(14)	0.0108(3)
Bi4	4*a*	0	0.95275(4)	0.40807(14)	0.0106(3)
Bi5	4*a*	0	0.29557(4)	0.56342(16)	0.0117(2)

[a]Hypothetical structural data. See text for details.
[b]U_{eq} is defined as one-third of the trace of the orthogonalized U_{ij} tensor.

Table 3
Selected interatomic distances for $Ce_2Rh_3Bi_5$[a]

	Distance (Å)		Distance (Å)
Ce1–Rh3 (× 2)	3.335(2)	Rh2–Bi1	2.751(2)
Ce1–Bi2 (× 2)	3.3015(15)	Rh2–Bi2 (× 2)	2.8000(15)
Ce1–Bi3 (× 2)	3.2940(14)	Rh2–Bi2	2.818(2)
Ce1–Bi5 (× 2)	3.2709(16)	Rh2–Bi5 (× 2)	2.8430(15)
		Rh2–Bi5	2.895(2)
Ce2–Rh1 (× 2)	3.196(2)		
Ce2–Rh1 (× 2)	3.467(2)	Rh3–Bi1 (× 2)	3.0361(19)
Ce2–Rh3	2.849(3)	Rh3–Bi3	2.787(3)
Ce2–Bi1 (× 2)	3.4765(13)	Rh3–Bi4 (× 2)	2.8416(18)
Ce2–Bi3	3.379(2)	Rh3–Bi5	2.758(3)
Ce2–Bi3	3.4175(19)		
Ce2–Bi4 (× 2)	3.4306(16)	Bi1–Bi4	3.2386(16)
		Bi1–Bi5 (× 2)	3.4984(12)
Rh1–Bi1	2.826(3)	Bi2–Bi3	3.2364(14)
Rh1–Bi3 (× 2)	2.6981(13)	Bi2–Bi5	3.1624(15)
Rh1–Bi4	2.780(3)	Bi2–Bi5 (× 2)	3.3093(11)
Rh1–Bi4	2.839(3)	Bi3–Bi1 (× 2)	3.6316(13)
		Bi3–Bi4 (× 2)	3.4263(11)

[a]Hypothetical structural data. See text for details.

3. Results and discussion

3.1. Structure

$Ce_2Rh_3(Pb,Bi)_5$ is a new representative of the orthorhombic $Y_2Rh_3Sn_5$ structure type [26]. Thus far, other members are limited to the $RE_2Rh_3Sn_5$ (RE = Y, Ce–Nd, Sm, Gd–Tm) family [10,26]. The La-analogue, however, forms with the orthorhombic $U_2Co_3Si_5$ (*Ibam*) structure [10]. Due to the similar covalent radii of Pb and Bi, atomic distances cannot be used to distinguish Pb from Bi. As shown in Fig. 1, $Ce_2Rh_3(Pb,Bi)_5$ possesses a rather complex quasi-two-dimensional structure, being built up of two-dimensional Rh-X (X = Pb/Bi) rings, which when stacked in the *a*-direction encapsulate Ce atoms in three-dimensional channels. This structure may be viewed alternatively as containing intergrown slabs of simpler structures (i.e., ternary ordering variants of $BaAl_4$), with structural motifs similar to the $Yb_2Pt_3Sn_5$ (*Pnma*) [27] and $Ce_2Au_3In_5$ ($Pmn2_1$) [25] structures. The differences in these three structures have been described as resulting from the ordering of the TX (T = Rh, Pt, Au; X = In, Sn) atoms within the polyanionic networks [25]. The Ce1, Ce2, Rh1, Rh2, Rh3, *X*1, *X*2, *X*3, *X*4 and *X*5 atoms of

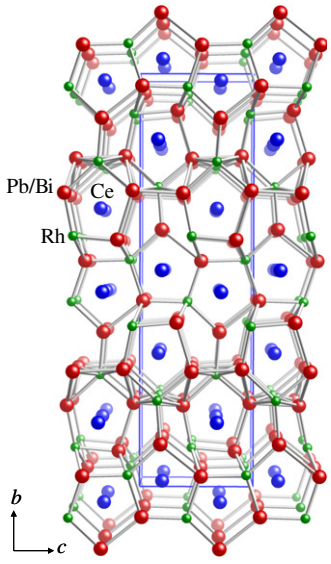

Fig. 1. Crystal structure of $Ce_2Rh_3(Pb,Bi)_5$ (Ce: medium isolated blue spheres, Rh: small green spheres, Pb/Bi: large red spheres) with unit cell outlined as a solid blue line. Bonds to the Ce atoms have been omitted for clarity.

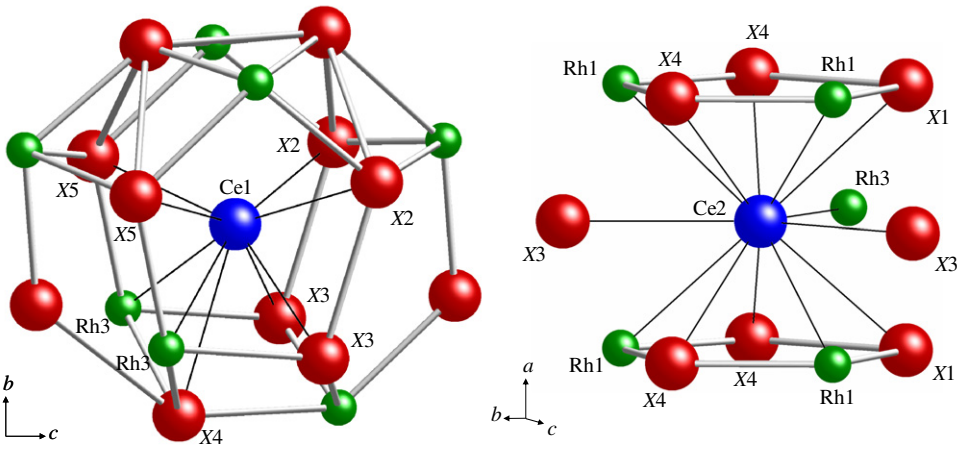

Fig. 2. Ce environments in $Ce_2Rh_3(Pb,Bi)_5$. Black lines depict the bonds to the Ce atoms. From electron microprobe analysis data, atoms labeled X are randomly occupied 80% by Pb and 20% by Bi atoms, yielding the composition $Ce_2Rh_3Pb_4Bi$.

$Ce_2Rh_3X_5$(X = Pb/Bi) all reside on inequivalent 4*a* crystallographic symmetry sites.

The Ce atoms have two different coordinations (see Table 3) which are illustrated in Fig. 2. Ce1 is 9-coordinate and bonds to two Rh3, two *X*2, two *X*3 and two *X*5 intra-planar atoms, and one *X*4 inter-planar atom. Ce2 is 13-coordinate with intra-planar bonds to four Rh1, four *X*4, and two *X*2 atoms, and inter-planar bonds to one Rh3, and two *X*3 atoms. In $Ce_2Rh_3(Pb,Bi)_5$, the Ce atoms reside in distorted pentagonal ([100] direction) and hexagonal ([001] direction) channels created by the Rh and Pb/Bi atoms. The shortest Ce···Ce distance in $Ce_2Rh_3(Pb,Bi)_5$ is 3.961 Å in [001], which is considerably longer than the 3.65 Å Ce–Ce bonds in *fcc* Ce [31], and above the Hill limit [32] of 3.40 Å for *f*-electron coupling.

The Rh and *X* (*X* = Pb/Bi) atoms form a complex three-dimensional $[Rh_3X_5]$ polyanion. This geometry may be viewed alternatively as stacked pentagonal and octagonal rings in the (200) plane. In the hypothetical $Ce_2Rh_3Bi_5$ structure (see Table 3), the Rh–Bi distances range from 2.6891(13) to 3.0361(19) Å. The average Rh–Bi distances are 2.786 Å (Rh1–Bi), 2.856 Å (Rh2–Bi) and 2.821 Å (Rh3–Bi), which are only slightly longer than the sum of the covalent radii of Rh and Bi of 2.77 Å [31]. The local coordination environments for the Rh atoms can be described as distorted monocapped trigonal prisms. For the Rh1 atom, the trigonal prism is made up of two Ce2, two *X*3 and two *X*4 atoms with a *X*1 capping atom. For Rh2, this geometry is formed by one *X*1 capping atom and three *X*2 and three *X*5 atoms. Rh3 atoms are bonded to two *X*1, one *X*3, two *X*4 and one *X*5 atoms with Ce2 as the capping atom. Bi–Bi distances (using bonding data from the solved $Ce_2Rh_3Bi_5$ structure) range from 3.1624(15) to 3.6316(13) Å with the shortest Bi–Bi distances between the Bi2 and Bi5 pairs in the octagonal rings. These distances are in agreement with those found in other intermetallic bismuthides [33].

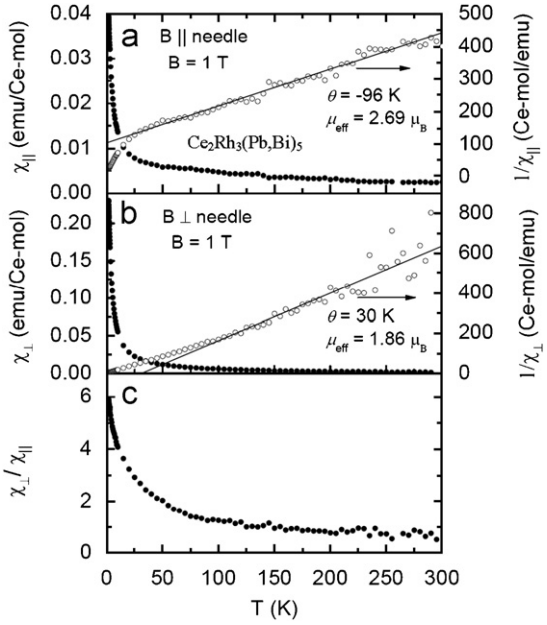

Fig. 3. The temperature dependence of the magnetic susceptibility (●) and the inverse magnetic susceptibility (○) for the magnetic field: (a) parallel ($\chi_{\parallel}$) and (b) perpendicular ($\chi_{\perp}$) to the needle axis of $Ce_2Rh_3(Pb,Bi)_5$ crystals. Solid lines indicate the best fit of the Curie–Weiss law (see text for details). (c) The temperature dependence of the ratio between $\chi_{\parallel}$ and $\chi_{\perp}$.

3.2. Physical properties

The magnetic susceptibility (χ) is shown in Fig. 3 for a $Ce_2Rh_3(Pb,Bi)_5$ single crystal measured in a field of 1 T both parallel (Fig. 3(a)) and perpendicular (Fig. 3(b)) to the needle axis. In both cases, the susceptibility increases monotonically with reduced temperature, and is well described by a Curie–Weiss law, at least at sufficiently high temperatures. Above 50 K in the parallel field configuration, the magnetic susceptibility is well described

by a Curie–Weiss law $\chi = C/(T-\theta)$, where the Curie constant C yields an effective moment of $2.7\,\mu_B$/Ce, very close to the Hund's rule value of $2.54\,\mu_B$/Ce. Here, the Weiss temperature $\theta = -96\,K$, signaling mean field interactions among these moments, which are antiferromagnetic and consistent with the enhancement of above the Curie–Weiss limit as the temperature drops below ~50 K. The situation is rather different when the field is applied perpendicular to the needle axis. Here, Curie–Weiss behavior is only observed above ~100 K, with a much smaller moment of $1.86\,\mu_B$/Ce and a net ferromagnetic Weiss field of 30 K, consistent with the suppression of χ below the Curie–Weiss law at the lowest temperatures. The ratio of $\chi_\perp/\chi_\parallel$ reaches values as large as 6 at 2 K (Fig. 3(c)), suggestive of substantial magneto-crystalline anisotropy. Such anisotropy is not unexpected, given the relatively low symmetry of the Ce sites, which is presumed to substantially lower the degeneracy of the Ce^{3+} quartet.

Measurements of the field dependence of the magnetization M shown in Fig. 4 find that M is increasingly nonlinear in fields perpendicular to the needle axis as the temperature is reduced (Fig. 4(b)). We interpret this as the normal paramagnetic behavior of individual Ce ions, where M is described by a Brillouin function, but do not rule out the possibility that part of the nonlinearity arises from fluctuations associated with incipient magnetic order. In contrast, the magnetization, $M_\parallel$, in the parallel field direction (Fig. 4(a)) is markedly less nonlinear with field for the same range of temperatures, while being substantially smaller than $M_\perp$. We conclude that the hard magnetic axis is along the needle axis. Taken together, our measurements of the magnetization find that $Ce_2Rh_3(Pb,Bi)_5$ is a system with highly localized Ce moments, where the magneto-crystalline anisotropy largely confines the moments to be along the needle axis. Further, the interactions among these moments, which we will show ultimately lead to magnetic order, are antiferromagnetic along the needle axis, but ferromagnetic in the transverse direction.

The heat capacity results are shown in Fig. 5. The magnetic part of the total heat capacity was estimated by fitting the data above 7 K to the Debye model, yielding a Debye temperature $\theta_D = 177\,K$. As shown in Fig. 5(a), the low temperature magnetic and electronic heat capacity is dominated by a sharp lambda-like anomaly, indicating the onset of magnetic order ~1.5 K. It is remarkable that the magnetic ordering temperature is almost two orders of magnitude smaller than the in-plane exchange interaction deduced from the Weiss temperature. This observation is consistent with a quasi-two-dimensional magnetic ordering, where magnetic order is driven by residual and weak interactions between planes of moments which are strongly coupled. The associated entropy is presented in Fig. 5(a); we see that the entropy difference between the ordered and paramagnetic state is very close to $R\ln 2$, as expected for Ce^{3+} ions. There is no evidence from the heat capacity for high-temperature Schottky anomalies, and indeed none are expected if the magnetic order involves a magnetic doublet ground state. Finally, C/T is presented in Fig. 5(a) to demonstrate that the magnetic order emerges from a Fermi-liquid-like state. For temperatures between 7 and 20 K, $C/T \sim \gamma \sim 30\,mJ\,Ce\text{-}mol^{-1}\,K^{-2}$, indicating (Fig. 5(a)

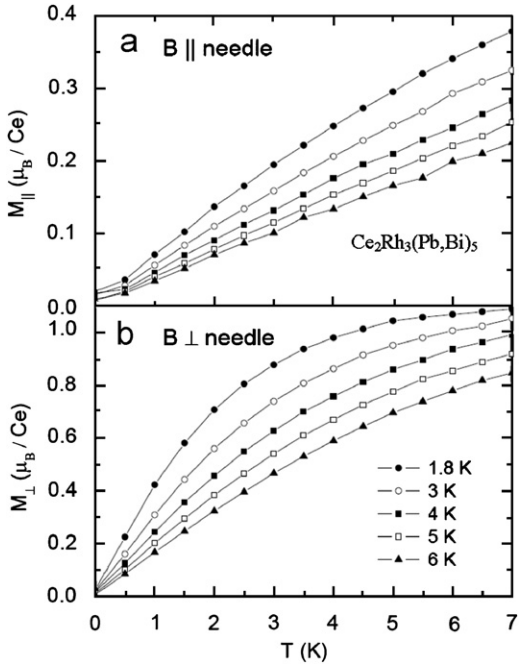

Fig. 4. The magnetic field dependence of the magnetization for the magnetic fields (a) parallel and (b) perpendicular to the needle axis for a $Ce_2Rh_3(Pb,Bi)_5$ crystal at $T = 1.8$, 3, 4, 5, and 6 K.

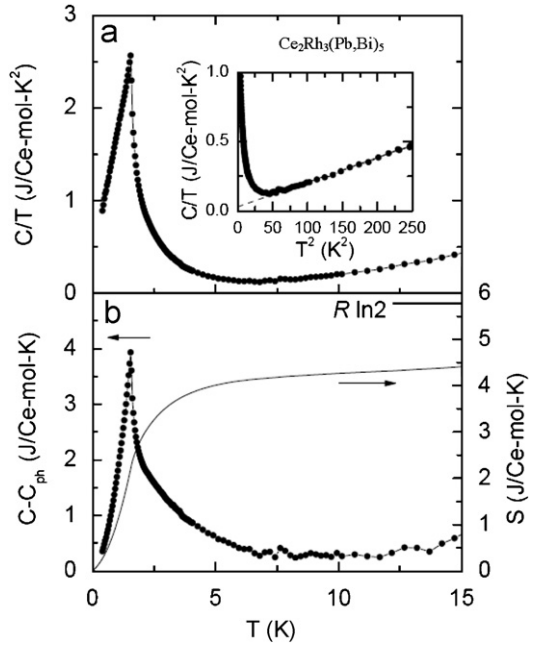

Fig. 5. (a) The temperature dependence of the specific heat (C) divided by temperature. The inset presents fitting results of data between 7 and 16 K to $C/T = \gamma + \beta T^2$. (b) The temperature dependence of the magnetic specific heat C–C_{ph} (●) and the entropy S (—).

inset) that the quasi-particles participating in this Fermi-liquid are only modestly enhanced by magnetic correlations. The heat capacity data are consistent with the ordering of well-localized Ce moments, and there is no indication of appreciable moment compensation via the Kondo effect.

The electrical resistivity (ρ) was measured with the current flowing along the needle axis, and with the magnetic field perpendicular to the current as shown in Fig. 6(a) for fields which range from 0 to 9 T. In all cases, the electrical resistivity is virtually temperature-independent between 2 and 40 K, although the resistivity is enhanced from its zero field value of 2.3 mΩ cm by the application of magnetic fields. A sharp drop is observed near 1.5 K, indicating the loss of spin disorder scattering at the magnetic ordering transition. An expanded view of the resistivity, measured in different magnetic fields, is presented in Fig. 6(b). It is clear that there is a sudden increase in the resistivity between 0 and 1.1 T. At higher fields, a distinct peak is observed in the resistance just above the magnetic ordering temperature, while the size of this peak and its temperature are shifted to higher temperatures with increased field. Finally, a substantial increase is observed at the lowest temperatures when fields larger than 3.2 T are applied.

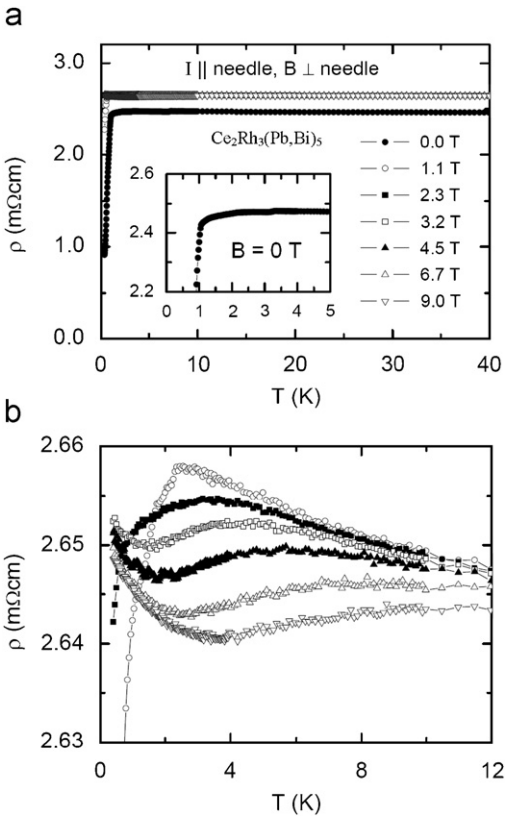

Fig. 6. (a) The temperature dependence of the resistivity ρ at temperatures below 40 K at various magnetic fields. The inset shows the plot of ρ vs. T below 5 K at 0 T. (b) Enlarged plot of ρ vs. T at magnetic fields below 12 K.

The temperature independence of the resistivity is remarkable, and would normally be explained as the signature of a dominant impurity scattering mechanism. The observations that the resistivity is halved with the onset of magnetic order, compounded with the extreme sharpness of the ordering transition in the heat capacity rules this explanation out, suggesting instead an unconventional electronic scattering mechanism such as those found in the so-called ''bad metals'', i.e., strongly correlated and magnetic systems such as $SrRuO_3$ [34] located near metal–insulator transitions. The development of the resistivity peak just above the ordering temperature is consistent with the superzone formation associated with antiferromagnetic order, and the accompanying elimination of parts of the Fermi surface. At least in low fields, much of the Fermi surface appears to survive, and the resistivity in the magnetically ordered state remains metallic. The data presented in Fig. 6(b) are consistent with the progressive elimination of the Fermi surface with magnetic ordering. We note that for a field intermediate between 2.3 and 3.2 T, the resistivity becomes purely insulating, i.e., increasing with decreasing temperature as $T \to 0$. The success which magnetic fields have in decimating the Fermi surface is suggestive that there is also strong electronic anisotropy in this system, and that this near-nesting stabilizes, if not enables, antiferromagnetic order. For all these reasons, the electrical resistivity data for $Ce_2Rh_3(Pb,Bi)_5$ are consistent with an antiferromagnetically ordered ground state.

4. Conclusions

Single crystals of non-centrosymmetric $Ce_2Rh_3(Pb,Bi)_5$ have been studied by means of single crystal X-ray diffraction, magnetic susceptibility, electrical resistivity and heat capacity measurements. The picture which emerges from the crystal structure and magnetic measurements is that of a quasi-two-dimensional system, having planes of well localized Ce moments with strong ferromagnetic coupling. Large magnetic anisotropy of the exchange couplings arises from the layered nature of the $Ce_2Rh_3(Pb,Bi)_5$ structure, where the Ce moments are more closely spaced within the planes and interact through the Rh-(Pb/Bi) channels. The moments themselves are largely perpendicular to the planes, contributing perhaps to interplanar coupling, which ultimately results in the antiferromagnetic order observed at 1.5 K. The electronic excitations also appear to be quasi-two-dimensional—a fact also supported by crystallographic evidence—perhaps leading to the nesting revealed by the temperature dependence of the resistivity. In zero field, the large magnitude of the resistivity and its near-temperature independence reveal that the carriers are almost localized in their quasi-two-dimensional environment. The destruction of the last vestiges of the Fermi surface is achieved using only modest magnetic fields, and yields a weakly localized yet still insulating ground state.

Acknowledgments

J.Y.C. acknowledges an NSF CAREER award (Grant DMR 0237664) and Alfred P. Sloan Fellowship for partial support of this project. Work at the University of Michigan (M.S.K., D.A.S., M.C.B., and M.C.A.) was supported by the National Science Foundation under Grant NSF-DMR-0405961. The electron-probe microanalysis was performed at the University of Michigan Electron Microbeam Analysis Laboratory (EMAL). The authors would like to thank Dixie P. Gautreaux (LSU, Chemistry) for her assistance with the structural data.

References

[1] B. Chevalier, T. Roisnel, J. Etourneau, J. Magn. Magn. Mater. 134 (1994) 88–94.
[2] A. Gil, M. Kolenda, S. Baran, B. Penc, M. Hofmann, A. Szytuła, Physica B 276 (2000) 742–743.
[3] R. Nirmala, A.V. Morozkin, M. Hofmann, V. Sankaranarayanan, K. Sethupathi, Y. Yamamoto, H. Hori, J. Alloys Compd. 335 (2002) 43–47.
[4] R. Nirmala, V. Sankaranarayanan, A.V. Morozkin, K. Sethupathi, J. Alloys Compd. 316 (2001) L1–L3.
[5] A. Szytuła, M. Kolenda, E. Ressouche, W. Sikora, J. Phys. Condens. Matter 9 (1997) 6651–6663.
[6] K.J. Proctor, K.A. Regan, A. Littman, F.J. DiSalvo, J. Alloys Compd. 292 (1999) 124–128.
[7] H.F. Braun, Phys. Lett. A 75 (1980) 386–388.
[8] Y. Singh, S. Ramakrishnan, Phys. Rev. B 69 (2004) Art. No. 174423.
[9] B. Chevalier, P. Lejay, J. Etourneau, M. Vlasse, P. Hagenmuller, Mater. Res. Bull. 17 (1982) 1211–1220.
[10] N.G. Patil, S. Ramakrishnan, Phys. Rev. B 59 (1999) 12054–12063.
[11] S. Noguchi, K. Okuda, Physica B 194 (1994) 1975–1976.
[12] C. Godart, L.C. Gupta, C.V. Tomy, S. Patil, R. Nagarajan, E. Beaurepaire, R. Vijayaraghavan, Physica B 163 (1990) 163–166.
[13] C. Mazumdar, R. Nagarajan, S.K. Dhar, L.C. Gupta, R. Vijayaraghavan, B.D. Padalia, Phys. Rev. B 46 (1992) 9009–9012.
[14] Y. Singh, S. Ramakrishnan, Z. Hossain, C. Geibel, Phys. Rev. B 66 (2002) Art. No. 014415.
[15] C. Mazumdar, A.K. Nigam, R. Nagarajan, C. Godart, L.C. Gupta, B.D. Padalia, G. Chandra, R. Vijayaraghavan, Appl. Phys. Lett. 68 (1996) 3647–3649.
[16] C. Mazumdar, A.K. Nigam, R. Nagarajan, L.C. Gupta, G. Chandra, B.D. Padalia, C. Godart, J. Appl. Phys. 81 (1997) 5781–5783.
[17] Z. Fisk, D.W. Hess, C.J. Pethick, D. Pines, J.L. Smith, J.D. Thompson, J.O. Willis, Science 239 (1988) 33–42.
[18] Z. Fisk, H.R. Ott, T.M. Rice, J.L. Smith, Nature 320 (1986) 124–129.
[19] Z. Fisk, J.L. Sarrao, J.L. Smith, J.D. Thompson, Proc. Natl. Acad. Sci. USA 92 (1995) 6663–6667.
[20] Y. Muro, K. Yamane, M.S. Kim, T. Takabatake, C. Godart, P. Rogl, J. Phys. Soc. Jpn. 72 (2003) 1745–1750.
[21] O.I. Bodak, B.Y. Kotur, V.I. Yarovets, E.I. Gladyshevskii, Sov. Phys. Crystallogr. 22 (1977) 385–388.
[22] L.G. Aksel'rud, Y.P. Yarmalyuk, E.I. Gladyshevskii, Kristallografiya 22 (1977) 861–863.
[23] B. Chabot, E. Parthé, J. Less-Common Met. 106 (1985) 53–59.
[24] Y. Singh, S. Ramakrishnan, Phys. Rev. B 68 (2003) Art. No. 054419.
[25] Y.V. Galadzhun, R.-D. Hoffmann, R. Pöttgen, M. Adam, J. Solid State Chem. 148 (1999) 425–432.
[26] M. Méot-Meyer, G. Venturini, B. Malaman, J. Steinmetz, B. Roques, Mater. Res. Bull. 19 (1984) 1181–1186.
[27] R. Pöttgen, A. Lang, R.D. Hoffmann, B. Künnen, G. Kotzyba, R. Müllmann, B.D. Mosel, C. Rosenhahn, Z. Kristallogr. 214 (1999) 143–150.
[28] R.H. Blessing, Acta Crystallogr. A5 (1995) 33.
[29] G.M. Sheldrick, in: SHELXL-97, Program for Refinement of Crystal Structures, University of Göttingen, Göttingen, Germany, 1997.
[30] A. Altomare, M.C. Burla, M. Camalli, G.L. Cascarno, A. Giacovazzo, A. Guagliardi, A.G.G. Moliterni, G. Polidori, R. Spagna, J. Appl. Cryst. 32 (1999) 115–119.
[31] R.D. Shannon, Acta Crystallogr. A 32 (1976) 751–767.
[32] H.H. Hill, Plutonium and Other Actinides, AIME, New York, 1970.
[33] A. Mar, Bismuthides, in: K.A. Gschneidner, J.-C.G. Bünzli, V.K. Pecharsky (Eds.), Handbook on the Physics and Chemistry of Rare Earths, vol. 36, Elsevier, Netherlands, 2006, pp. 1–82.
[34] L. Klein, J.S. Dodge, C.H. Ahn, G.J. Snyder, T.H. Geballe, M.R. Beasley, A. Kapitulnik, Phys. Rev. Lett. 77 (1996) 2774–2777.